

Uncertainty-Aware Deep Learning for Automated Skin Cancer Classification: A Comprehensive Evaluation

Hamzeh Asgharnezhad^a, Pegah Tabarisaadi^a, Abbas Khosravi^a, Roohallah Alizadehsani^a, U. Rajendra Acharya^b

^aDeakin University, Australia (e-mail: abbas.khosravi@deakin.edu.au),

^bSchool of Mathematics, Physics and Computing University of Southern Queensland Toowoomba QLD Australia

Abstract

Accurate and reliable skin cancer diagnosis is critical for early treatment and improved patient outcomes. Deep learning (DL) models have shown promise in automating skin cancer classification, but their performance can be limited by data scarcity and a lack of uncertainty awareness. In this study, we present a comprehensive evaluation of DL-based skin lesion classification using transfer learning and uncertainty quantification (UQ) on the HAM10000 dataset. In the first phase, we benchmarked several pre-trained feature extractors—including Contrastive Language–Image Pretraining (CLIP) variants, Residual Network-50 (ResNet50), Densely Connected Convolutional Network (DenseNet121), Visual Geometry Group network (VGG16), and EfficientNet-V2-Large—combined with a range of traditional classifiers such as Support Vector Machine (SVM), eXtreme Gradient Boosting (XGBoost), and logistic regression. Our results show that CLIP-based vision transformers, particularly LAION CLIP ViT-H/14 with SVM, deliver the highest classification performance. In the second phase, we incorporated UQ using Monte Carlo Dropout (MCD), Ensemble, and Ensemble Monte Carlo Dropout (EMCD) to assess not only prediction accuracy but also the reliability of model outputs. We evaluated these models using uncertainty-aware metrics such as uncertainty accuracy (UAcc), uncertainty sensitivity (USen), uncertainty specificity (USpe), and uncertainty precision (UPre). The results demonstrate that ensemble methods offer a good trade-off between accuracy and uncertainty handling, while EMCD is more sensitive to uncertain predictions. This study highlights the importance of integrating UQ into DL-based medical diagnosis to enhance both performance and trustworthiness in real-world clinical applications.

Keywords: Deep Learning, Machine Learning, Classification, Skin cancer

1. Introduction

Skin cancer is one of the most prevalent types of cancer worldwide, with its incidence rising significantly over the past decades. This increase is potentially linked to lifestyle changes and environmental factors such as ozone layer depletion [1]. Skin cancer primarily results from abnormal growth of skin cells and is categorized into two main types: melanoma and non-melanoma. While non-melanoma is more common and has a lower mortality rate, melanoma is responsible for nearly 75% of skin cancer-related deaths [2]. In 2018, approximately 300,000 new cases of melanoma and over one million cases of non-melanoma were reported globally. Given current trends, these numbers are expected to rise substantially in the next two decades, making skin cancer a growing public health concern [3].

Early diagnosis of skin cancer is crucial for improving survival rates and treatment outcomes. For instance, in the United States, the five-year survival rate for localized melanoma is 98.4%, while for metastatic melanoma, it drops drastically to 22.5%. The low mortality rate of non-melanoma skin cancer, at 0.64 deaths per 100,000 cases, further highlights the importance of early detection [4]. However, diagnosing skin cancer remains a challenge, even for experienced dermatologists, as it requires careful analysis of dermatologist spot images. Given the projected increase in cases, relying solely on manual examination

is not sustainable. Therefore, advanced diagnostic tools, such as artificial intelligence-based methods, are becoming increasingly essential to support healthcare professionals, enhance diagnostic accuracy, and reduce the burden on the medical system.

DL algorithms have emerged as powerful tools for skin cancer detection, offering significant improvements in accuracy, efficiency, and scalability compared to traditional diagnostic methods [5, 6, 7]. Convolutional Neural Networks (CNNs), particularly, have demonstrated exceptional performance in analyzing dermatologist spot images by automatically learning complex patterns and distinguishing between malignant and benign lesions. These models can process large-scale datasets and extract hierarchical features that might be imperceptible to human experts, thus improving diagnostic reliability. Studies have shown that DL-based systems can achieve dermatologist-level performance in skin cancer classification, reducing the risk of misdiagnosis and enabling early detection, which is critical for successful treatment [3, 4].

Deep neural networks (DNNs) can struggle with unseen or ambiguous medical cases, potentially leading to incorrect diagnoses that may put patients at risk [8]. This limitation arises from their black-box nature, as they produce predictions without conveying the confidence behind them [9]. In medical diagnosis, particularly for critical conditions like skin cancer, understanding uncertainty is essential, as even a small misjudgment can

have serious consequences. UQ helps bridge this gap by allowing AI models to estimate and communicate their confidence levels, empowering healthcare professionals to assess the reliability of predictions. By incorporating UQ, medical AI systems can prioritize uncertain cases for further evaluation, minimize diagnostic errors, and enhance transparency, ultimately improving patient safety and trust in automated diagnosis.

DL models require large amounts of labeled data to achieve high accuracy. However, obtaining such datasets in the medical domain remains a significant challenge [10, 11, 12]. Unlike general computer vision tasks where massive labeled datasets are readily available, medical imaging datasets are often limited in size. Labeling medical data is not only time-consuming but also expensive, as it requires expert annotation from professionals [13]. Moreover, DNNs consist of thousands of parameters that must be optimized, and training them from scratch requires substantial computational resources and time. In fields like dermatology, the scarcity of labeled medical images further complicates training, increasing the risk of overfitting. These challenges emphasize the need for techniques to efficiently leverage limited data while ensuring high diagnostic performance.

One effective approach to overcoming the challenges of training deep learning models on limited medical datasets is transfer learning [14, 15]. Instead of training a model from scratch, transfer learning leverages pre-trained networks that have already learned rich and generalizable features from large-scale datasets [16]. These networks, trained initially on diverse image collections, can be fine-tuned or adapted to specific tasks, such as skin cancer detection, where labeled data is often scarce. By reusing learned representations, transfer learning significantly reduces computational costs, accelerates training, and enhances model generalization, making deep learning a feasible and effective solution for medical image analysis.

Several well-established transfer learning models have been widely used for image analysis due to their strong feature extraction capabilities. ResNet50 [17] is known for its deep residual connections that improve gradient flow and allow the training of very deep networks. DenseNet121 [18] enhances feature propagation by densely connecting layers, leading to efficient parameter utilization. VGG16 [19], despite being an older architecture, remains popular due to its simple yet effective design. EfficientNet-V2-L [20] builds upon compound scaling to optimize model size and performance, making it highly efficient for medical imaging tasks. CLIP [21], a more recent approach, introduces contrastive learning with text-image supervision, potentially enabling a broader and more generalizable feature representation. These models differ in architectural depth, parameter efficiency, and feature extraction methods, which influence their suitability for specific tasks.

In this study, we explore the effectiveness of vision transformers for automated skin cancer classification through transfer learning. Specifically, we utilize pre-trained transformer-based models, including various CLIP architectures, to extract deep features from skin cancer images. These are compared against traditional convolutional neural network (CNN) feature extractors such as ResNet50, DenseNet121, VGG16, and EfficientNet-V2-L. Our goal is to assess the feature representation capability

of vision transformers compared to CNNs and identify which architecture provides more discriminative information for classifying different types of skin cancer. To the best of the authors' knowledge, this is the first study to investigate the application of CLIP-based vision transformers for feature extraction in automated skin cancer classification.

To classify the extracted features, we evaluate multiple machine learning classifiers, including Support Vector Machine, Extreme Gradient Boosting, K-Nearest Neighbors, Logistic Regression, Random Forest, Gradient Boosting, Decision Tree, and Naive Bayes. This diverse set of classifiers allows us to analyze the effectiveness of different learning paradigms and their impact on classification performance. By conducting a comparative analysis, we seek to identify the most suitable feature-classifier combination for skin cancer detection.

Beyond classification accuracy, uncertainty estimation is a critical aspect of medical AI applications. To ensure reliability in automated diagnosis, we integrate UQ by employing a neural network-based classifier with uncertainty-aware mechanisms. Techniques such as model ensembles [22], MCD [23], and EMCD are used to estimate predictive uncertainty, helping to assess confidence levels in model outputs. This aspect is particularly important in clinical decision-making, where incorrect predictions can have significant consequences.

By incorporating transfer learning, machine learning-based classification, and UQ, this study provides a comprehensive evaluation of deep learning-based skin cancer diagnosis. Unlike prior research, which often focuses solely on classification performance, our work emphasizes the importance of uncertainty estimation in improving the trustworthiness of automated medical diagnosis. This approach aims to bridge the gap between model accuracy and real-world applicability, ensuring that AI-driven skin cancer detection can be both effective and reliable. The main contributions of this paper are as follows:

- A first-of-its-kind comparative analysis of CLIP-based vision transformers and CNN-based models for feature extraction in automated skin cancer classification.
- Evaluation of a diverse set of machine learning classifiers on features extracted from both vision transformers and CNNs to determine the most effective feature-classifier combinations.
- Integration of uncertainty quantification into the classification pipeline using neural network-based models to support more reliable diagnostic outputs.
- Comprehensive comparison of uncertainty estimation techniques, including Monte Carlo Dropout, Deep Ensembles, and Ensemble MCD, in the context of skin cancer image classification.

The remainder of this paper is organized as follows. Section 2 provides an overview of the transfer learning models and machine learning classifiers employed in this study, along with a detailed explanation of the uncertainty quantification methods and evaluation metrics used to assess prediction confidence. Section 3 introduces the HAM10000 dataset and presents a

comprehensive experimental analysis, including performance comparisons across different feature extractor–classifier combinations and uncertainty-aware methods. Finally, Section 4 summarizes the key findings and discusses their implications for reliable and trustworthy automated skin cancer diagnosis.

2. Background

2.1. CLIP

CLIP (Contrastive Language-Image Pre-training) is a vision model developed by OpenAI that learns transferable visual representations from natural language supervision [21]. Unlike traditional computer vision models trained on predefined object categories with labeled datasets, CLIP leverages large-scale natural language supervision by associating images with textual descriptions. The model is trained using a contrastive objective, where it learns to match an image with its corresponding textual description from a large dataset of (image, text) pairs. This approach enables CLIP to understand and generalize to various visual concepts without the need for dataset-specific fine-tuning. As a result, CLIP can perform zero-shot learning, meaning it can classify images into new categories based on text descriptions alone, without requiring additional labeled training data.

One of the key distinctions of CLIP from other pretrained algorithms, such as those trained on ImageNet, is its reliance on internet-scale text-image pairs rather than manually labeled datasets. The training dataset for CLIP consists of 400 million (image, text) pairs collected from the internet, referred to as WebImageText (WIT). This dataset is significantly larger and more diverse than conventional computer vision training datasets like ImageNet, which typically contain only a fixed set of labeled classes. The contrastive training objective allows CLIP to develop a broad understanding of visual concepts, enabling it to perform well across various tasks, including optical character recognition (OCR), action recognition, and fine-grained object classification. Moreover, CLIP exhibits enhanced robustness to natural distribution shifts, making it more reliable in real-world applications where image distributions may differ from those in standard benchmark datasets.

CLIP effectiveness is demonstrated by its ability to perform competitively across a wide range of computer vision tasks without requiring additional fine-tuning. It achieves results comparable to fully supervised models on ImageNet while also transferring effectively to over 30 different benchmarks, including those involving object classification, scene recognition, and image retrieval. Its zero-shot capabilities allow it to classify images based on textual descriptions alone, making it highly adaptable to new tasks without the need for manually labeled training data. Additionally, CLIP exhibits strong robustness to domain shifts, maintaining better performance than traditional models when tested on datasets with natural variations. This adaptability, combined with its large-scale training approach, highlights its potential as a versatile tool for general-purpose vision applications.

2.2. EfficientNetV2

EfficientNetV2 [20] is an improved convolutional network designed for faster training and better parameter efficiency compared to its predecessor, EfficientNet. It leverages training-aware neural architecture search and progressive learning to optimize training speed while maintaining high accuracy. A key innovation is the introduction of Fused-MBConv layers, which replace depthwise convolutions in early network stages to enhance computational efficiency. Unlike the original EfficientNet, which scaled depth, width, and resolution uniformly, EfficientNetV2 applies non-uniform scaling to allocate resources more effectively. These improvements result in models that train up to $11\times$ faster and use $6.8\times$ fewer parameters, making them highly suitable for real-world applications with limited computational resources.

EfficientNetV2 has been extensively trained on large-scale datasets, including ImageNet ILSVRC2012 (1.28 million images, 1,000 classes) and ImageNet21k (13 million images, 21,841 classes). Pretraining on ImageNet21k provides a substantial boost in generalization, allowing EfficientNetV2 to achieve 87.3% top-1 accuracy on ImageNet ILSVRC2012 while maintaining computational efficiency. Beyond large-scale datasets, EfficientNetV2 has been tested on multiple transfer learning benchmarks, such as CIFAR-10, CIFAR-100, Flowers, and Cars, where it consistently outperforms prior models. The model ability to generalize well across different datasets highlights its robustness and adaptability in various domains, from everyday object classification to fine-grained recognition tasks.

Compared to other state-of-the-art models, such as ResNeSt, NFNets, and Vision Transformers (ViTs), EfficientNetV2 strikes a superior balance between accuracy, parameter size, and training speed. While ViTs have demonstrated strong performance on large datasets, they require extensive computational resources and long training times. In contrast, EfficientNetV2 achieves similar or better accuracy while training $5\times$ – $11\times$ faster. Compared to NFNets and other convolutional architectures, EfficientNetV2 reduces training bottlenecks by dynamically adjusting image size and regularization strength, ensuring both efficiency and accuracy. These features make EfficientNetV2 a powerful choice for deep learning applications that require high performance with optimized resource utilization.

2.3. Predictive Uncertainty Quantification

Uncertainty quantification (UQ) plays a critical role in the deployment of machine learning models, particularly in high-stakes and real-world scenarios. While traditional models provide point predictions, they cannot often express their confidence in those outputs. This becomes problematic when models encounter unfamiliar, noisy, or ambiguous data, which are—common occurrences in practical applications. Without a reliable measure of uncertainty, users may blindly trust predictions, potentially leading to harmful or costly decisions. UQ addresses this gap by offering insights into the model confidence, enabling more informed decision-making, risk management, and system robustness. It allows stakeholders to identify when a prediction may be unreliable, trigger human oversight when needed, and even

improve downstream processes by incorporating confidence levels into decision pipelines. Ultimately, integrating UQ not only enhances model transparency and trustworthiness but also helps bridge the gap between theoretical performance and real-world reliability.

In uncertainty-aware classification, it is often useful to define a threshold that separates predictions into certain and uncertain categories based on their associated uncertainty scores. This threshold enables practitioners to interpret the model’s outputs not only in terms of class labels but also in terms of how confident the model is in its decisions. Once this division is made, each prediction can be categorized into one of four groups: Correct and Certain (CC), Incorrect and Uncertain (IU), Correct and Uncertain (CU), and Incorrect and Certain (IC) [24].

Ideally, a well-calibrated model should produce as many predictions as possible in the CC group, where the model is both correct and confident. The next desirable outcome is IU, where the model makes an error but acknowledges its uncertainty. This behavior is useful because it alerts the user to potential issues in the prediction, thereby preventing over-reliance on incorrect outputs. On the other hand, predictions in the CU category are less problematic but still suboptimal, as the model correctly classifies the input but lacks confidence in its own decision. The most undesirable group is IC, where the model makes a wrong prediction with high confidence—these cases are the most dangerous in real-world applications, as they may mislead users into making incorrect decisions with undue trust in the model. To quantitatively evaluate the quality of uncertainty estimation, several metrics have been proposed based on these four groups.

2.4. Monte Carlo Dropout (MCD)

Monte Carlo Dropout is a widely adopted method for approximating Bayesian inference in neural networks. It addresses the challenge of computing the posterior distribution over model weights by using dropout not only during training but also at inference time, as proposed by Gal and Ghahramani [23]. This approach enables the network to produce multiple outputs by performing stochastic forward passes with randomly dropped neurons, effectively generating samples from an approximate posterior.

Given an input x , the mean prediction across T such stochastic passes is given by:

$$\mu_{\text{pred}} \approx \frac{1}{T} \sum_{t=1}^T p(y = c \mid x, \hat{\omega}_t) \quad (1)$$

where $p(y = c \mid x, \hat{\omega}_t)$ denotes the softmax probability for class c obtained from the t -th forward pass using the sampled weights $\hat{\omega}_t$.

This method also supports the quantification of model uncertainty. A common measure is *predictive entropy*, which evaluates the spread of the averaged class probabilities [23]:

$$PE = - \sum_c \mu_{\text{pred}} \log \mu_{\text{pred}} \quad (2)$$

where the sum is over all possible output classes c . Lower entropy indicates higher confidence in the prediction, while higher

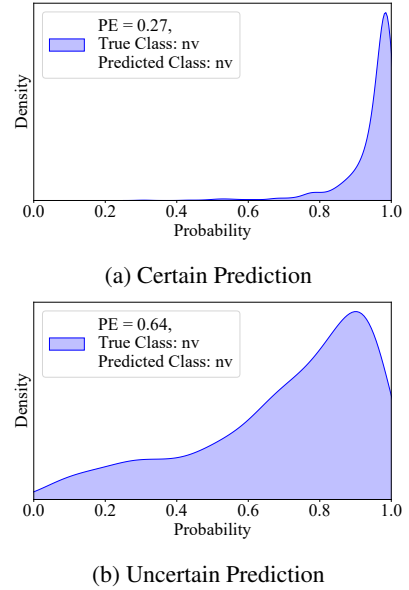


Figure 1: Comparison of Probability Density: Certain vs. Uncertain for test sample of class Nevus (LAION CLIP ViT-H/14 + MCD)

entropy suggests greater uncertainty. This makes the metric particularly useful for identifying ambiguous or potentially unreliable predictions in classification tasks.

Figure 1 illustrates the probability density distributions for two test samples classified as belonging to the Nevus class using the LAION CLIP ViT-H/14 model with Monte Carlo Dropout (MCD). Subfigure 1a depicts a confident prediction, where the distribution is sharply peaked around the predicted class, indicating low uncertainty. In contrast, Subfigure 1b shows a broader, flatter distribution, reflecting greater epistemic uncertainty in the model prediction.

2.5. Deep Ensembles

Deep ensembles provide a practical and effective means for estimating uncertainty by leveraging the diversity among multiple independently trained neural networks. Instead of relying on Bayesian inference, this method trains N separate models using different random initializations and, optionally, varied data sampling strategies such as shuffling or bootstrapping [22]. The variation in their learned parameters allows the ensemble to capture epistemic uncertainty through differences in model predictions.

For a given input x , each ensemble member generates a predictive distribution $p_{\theta_i}(y|x)$, where θ_i denotes the parameters of the i -th model. The aggregated predictive distribution across the ensemble is calculated as:

$$\hat{p}(y|x) = \frac{1}{N} \sum_{i=1}^N p_{\theta_i}(y|x) \quad (3)$$

To assess the uncertainty in the prediction, predictive entropy (PE) can be computed as:

$$PE = - \sum_{i=1}^C \hat{p}(y_i|x) \log \hat{p}(y_i|x) \quad (4)$$

where C is the number of classes in the classification task. A low entropy score corresponds to confident predictions, whereas a high entropy value signals uncertainty. As shown in the work by Lakshminarayanan et al. [22], this technique yields reliable and well-calibrated predictions without the need for complex Bayesian methods.

2.6. Ensemble Monte Carlo Dropout (EMCD)

Ensemble Monte Carlo Dropout (EMCD) is a hybrid strategy that merges the strengths of deep ensembles and Monte Carlo Dropout to enhance uncertainty estimation. In this method, N separate neural networks are trained independently, as done in traditional ensembles. At inference time, each model generates T stochastic predictions by applying dropout, similar to the Monte Carlo Dropout procedure.

For a test sample x , the i^{th} model produces its predictive distribution by averaging the outputs from T dropout-enabled forward passes:

$$\hat{p}_{\theta_i}(y|x) = \frac{1}{T} \sum_{t=1}^T p_{\theta_i}(y|x) \quad (5)$$

where $p_{\theta_i}(y|x)$ refers to the softmax output obtained during the t^{th} stochastic pass using a distinct dropout mask within the i^{th} model.

To obtain the final predictive distribution from the EMCD model, the averaged outputs of all N models are combined:

$$\hat{p}(y|x) = \frac{1}{N} \sum_{i=1}^N \hat{p}_{\theta_i}(y|x) \quad (6)$$

The associated uncertainty can be quantified using predictive entropy:

$$PE = - \sum_{i=1}^C \hat{p}(y_i|x) \log \hat{p}(y_i|x) \quad (7)$$

where C represents the number of possible output classes. By integrating the model diversity introduced by ensembles with the randomness of dropout-based sampling, EMCD captures a richer representation of epistemic uncertainty and often leads to more calibrated predictions.

2.7. Uncertainty Confusion Matrix

The uncertainty confusion matrix [24], inspired by the traditional confusion matrix, is presented in Table 1. This matrix categorizes predictions based on both correctness (correct or incorrect) and the model’s confidence level (certain or uncertain). Ideally, an uncertainty-aware model should concentrate its predictions in the Correct and Certain (CC) and Incorrect and Uncertain (IU) categories, which are highlighted in green. These outcomes indicate confident correct predictions and cautious behavior when uncertain, respectively—both are desirable

Table 1: Uncertainty confusion matrix

		Correctness	
		Correct	Incorrect
Confidence	Certain	CC	IC
	Uncertain	CU	IU

for safe and reliable decision-making. In contrast, predictions falling into the Incorrect and Certain (IC) and Correct and Uncertain (CU) categories (highlighted in red) are less favorable, particularly IC, which represents confident errors that may lead to misleading conclusions in real-world applications.

Uncertainty Sensitivity

Uncertainty Sensitivity (USen) is a key metric used to evaluate the effectiveness of a model uncertainty estimation. Specifically, it quantifies the model ability to recognize its own incorrect predictions as uncertain. In uncertainty-aware classification, this is highly desirable, as it ensures that erroneous predictions are accompanied by appropriate caution, thereby reducing the risk of overconfident failures in deployment.

The metric is defined as the proportion of incorrect predictions that the model also labels as uncertain. A higher value of U_{sen} indicates better sensitivity to uncertainty in erroneous cases.

$$USen = \frac{N_{IU}}{N_{IC} + N_{IU}} \quad (8)$$

where N_{IU} is the number of predictions that are both Incorrect and Uncertain, and $N_{incorrect}$ is the total number of Incorrect predictions made by the model.

Uncertainty Specificity

Uncertainty Specificity (USpe) evaluates the model’s ability to assign low uncertainty to its correct predictions. This metric reflects how confidently the model identifies its accurate outputs. In an ideal scenario, correct predictions should also be accompanied by high certainty, ensuring that the model confidence aligns with its correctness.

USpe is calculated as the proportion of predictions that are both Correct and Certain out of all Correct predictions made by the model.

$$USpe = \frac{N_{CC}}{N_{CC} + N_{CU}} \quad (9)$$

where N_{CC} denotes the number of Correct and Certain predictions, and N_{CU} is the number of Correct and Uncertain predictions.

Uncertainty Precision

Uncertainty Precision (UPre) measures how precise the model is in associating uncertainty with incorrect predictions. It indicates the proportion of uncertain predictions that are actually incorrect, helping to assess whether the model’s uncertainty estimates are meaningfully targeted at potentially erroneous outputs.

UPre is defined as the ratio of Incorrect and Uncertain predictions to the total number of Uncertain predictions:

$$UPre = \frac{N_{IU}}{N_{CU} + N_{IU}} \quad (10)$$

where N_{IU} is the number of Incorrect and Uncertain predictions, and N_{CU} is the number of Correct and Uncertain predictions.

Uncertainty Accuracy

Uncertainty Accuracy (UAcc) provides an overall measure of how well the model aligns its uncertainty estimates with prediction correctness. Specifically, it captures the proportion of predictions that fall into the desired categories: either Correct and Certain (CC) or Incorrect and Uncertain (IU). These are considered ideal outcomes, where the model is confident when correct and cautious when wrong.

UAcc is calculated as the ratio of these desirable predictions to the total number of predictions made:

$$UAcc = \frac{N_{CC} + N_{IU}}{N_{CC} + N_{CU} + N_{IU} + N_{IC}} \quad (11)$$

where N_{CC} denotes the number of Correct and Certain predictions, N_{IU} is the number of Incorrect and Uncertain predictions, and N_{CU} is the number of correct and uncertain predictions and N_{IC} is the number of incorrect and uncertain predictions made by the model.

3. Simulation Results and Discussions

In this section, the proposed algorithm is applied to real-world datasets, and the performances of different algorithms are compared from different perspectives.

3.1. Dataset

The HAM10000 dataset [25], short for 'Human Against Machine with 10000 training images', is a widely recognized resource for research in dermatological image analysis, especially in the development of machine learning models for skin lesion classification. It was compiled by researchers at the Medical University of Vienna and the Australian Skin Cancer Research Institute to provide a comprehensive and diverse collection of dermatoscopic images that reflect real-world clinical conditions. The dataset contains 10,015 dermatoscopic images representing seven types of pigmented skin lesions. These include melanocytic nevi (nv), melanoma (mel), benign keratosis-like lesions (bkl), basal cell carcinoma (bcc), actinic keratoses and intraepithelial carcinoma (akiec), vascular lesions (vasc), and dermatofibroma (df). Alongside the images, metadata such as the patient's age, sex, and lesion location are also provided, enabling the development of more nuanced and context-aware diagnostic models. One of the strengths of HAM10000 is the variability in its sources. The images were gathered from two different geographic and clinical settings—Austria and Australia—using a range of dermatoscopic devices. This diversity makes the dataset particularly useful for training models that need to generalize well across different patient populations and imaging environments.

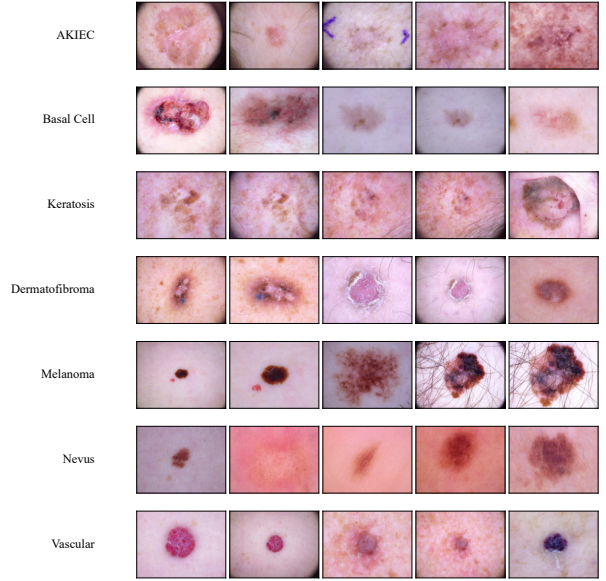


Figure 2: Examples of skin lesions from HAM10000 Dataset.

HAM10000 has become a foundational dataset in automated skin cancer detection and was prominently featured in the ISIC (International Skin Imaging Collaboration) 2018 challenge. It continues to support research in deep learning, uncertainty quantification, and explainable AI by providing a large, high-quality dataset that captures the complexity of dermatological diagnosis.

Figure 2 illustrates the distribution of lesion types across the seven diagnostic categories included in the HAM10000 dataset. These classes are: Nevus, Melanoma, Keratosis, Basal Cell, AKIEC, Vascular and Dermatofibroma.

3.2. Proposed Method

The proposed method, as illustrated figure 3, begins with the HAM10000 dataset, which provides skin cancer images as input. These images are passed through a CLIP-based vision transformer that functions as a feature extractor. Following this, three uncertainty estimation methods (MCD, Ensemble and EMCD) are applied to quantify the predictive uncertainty. Finally, a comparison metric Uncertainty Accuracy (UAcc) is used to evaluate and compare the performance of the proposed methods with other approaches.

3.3. Results

To identify a strong baseline for skin lesion classification using the HAM10000 dataset, we conducted a comprehensive experimental comparison of state-of-the-art transfer learning feature extractors combined with various traditional machine learning classifiers. The goal was to evaluate the effectiveness of different visual representation models, including CLIP-based vision transformers, convolutional neural networks, and EfficientNet variants, when used as fixed feature extractors. These extracted features were first reduced to 100 dimensions using Principal Component Analysis (PCA) [26] and then passed to

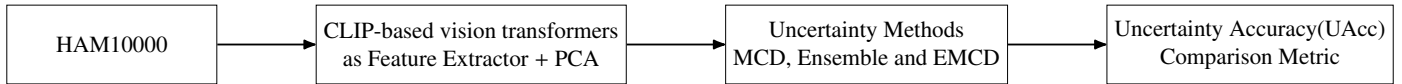


Figure 3: Architecture of the proposed method

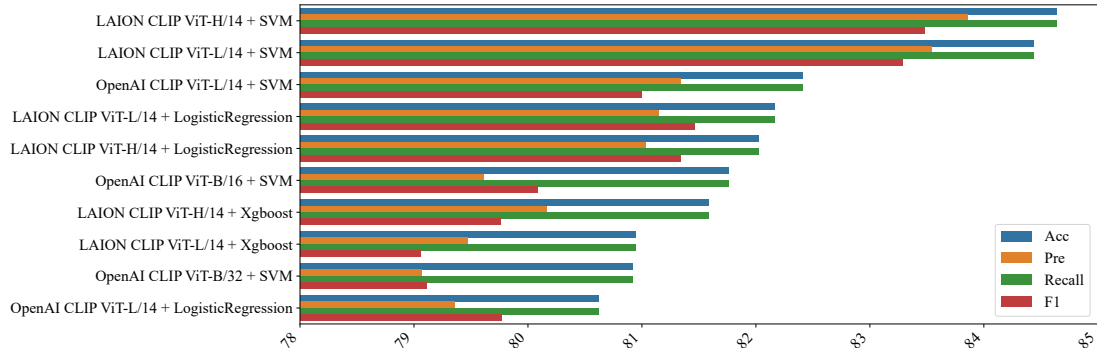


Figure 4: Performance comparison of the best-performing combinations of feature extractors and classifiers. Evaluation done based on Accuracy (Acc), Precision (Pre), Recall, and F1 Score (F1). The results reflect the impact of CLIP and ResNet-based extractors paired with classifiers such as SVM, XGBoost, k-Nearest Neighbors, and Logistic Regression.

standard classifiers such as support vector machines (SVM), logistic regression, k-nearest neighbors, decision trees, random forests, XGBoost, gradient boosting, and naive Bayes. All models were evaluated using key metrics including accuracy, precision, recall, and F1 Score (F1).

Table 3 presents the mean results obtained from 10 independent runs of each algorithm to ensure robustness and account for variability in training. Figure 4 visualizes the performance of the top-performing combinations of feature extractors and classifiers across key metrics. This summary plot facilitates a comparative view of the most effective algorithmic setups for skin lesion classification. The results demonstrate consistent trends across combinations. Notably, the LAION CLIP ViT-H/14 feature extractor paired with an SVM classifier achieved the highest overall performance, with an average accuracy of 84.64%, precision of 83.86%, recall of 84.64%, and F1 of 83.48. These findings highlight the strength of CLIP-based vision transformers—particularly those pre-trained on large and diverse datasets like LAION—in generating highly discriminative features for medical image classification tasks such as skin lesion detection.

In general, SVM and tree-based classifiers such as XGBoost and LogisticRegression provided strong results across classifiers. On the other hand, classifiers such as naive Bayes, decision trees, and k-nearest neighbors tended to yield lower performance, particularly when paired with deep feature extractors like EfficientNet-V2-L. This is likely due to a mismatch between the complexity of the feature space and the capacity of these simpler models to model decision boundaries effectively.

Interestingly, although EfficientNet-V2-L is known for its performance in standard image classification tasks, it underperformed in this setting, especially when used with basic classifiers. This highlights the importance of not only the feature extractor but also its alignment with the downstream classifier. In con-

clusion, our experiments demonstrate that CLIP-based vision transformers, especially the ViT-H/14 variant, offer a powerful foundation for skin cancer classification when combined with suitable classifiers like SVM.

In the second phase of our study, we extended our baseline experiments by incorporating uncertainty quantification into the classification pipeline. Building on the previously evaluated feature extractors, we applied three widely-used uncertainty-aware techniques: Monte Carlo Dropout (MCD), Ensemble, and Ensemble Monte Carlo Dropout (EMCD). We employed a custom neural network architecture, consisting of two hidden layers with 64 and 16 neurons respectively and ReLU activations, intermediate dropout layers to enable stochastic behavior during inference, and an output layer for classification. For the Ensemble and EMCD methods, six instances of this model were trained independently using different random weight initializations to capture model uncertainty. These methods were combined with various deep feature extractors to analyze not only classification performance but also the model’s behavior under uncertainty. The goal was to assess both predictive accuracy and the model’s ability to express and handle uncertainty in its outputs, which is particularly important for high-stakes applications like medical diagnosis.

Each uncertainty-aware method was applied to the extracted features without retraining the feature extractor. The classifier in each case was adapted to support uncertainty estimation. In addition to the standard evaluation metrics such as accuracy, precision, recall, and F1, we included several uncertainty-specific metrics: the number of correct and certain predictions (CC), Incorrect and certain predictions (IC), correct and uncertain predictions (CU), and Incorrect and uncertain predictions (IU), as well as uncertainty accuracy, uncertainty sensitivity, uncertainty specificity, and uncertainty precision. These metrics help us understand not just how accurate a model is, but also how well

it knows when it is uncertain.

The results presented in Table 2 represent the mean performance over 10 independent runs for each model. Figure 5 illustrates the performance of the top uncertainty-aware models across F1 and Uncertainty Accuracy, highlighting the most effective combinations of feature extractors and uncertainty quantification techniques. These results show that the ensemble method, when applied to LAION CLIP ViT-H/14, achieved the highest classification uncertainty accuracy (UAcc = 78.53%), along with accuracy (84.17%), precision (83.46%), and recall (84.17%) values that remained consistent and balanced. It also produced the highest average number of correct and certain predictions (CC = 1305), indicating reliable confidence in correct classifications. Although these uncertainty-aware methods did not exceed the non-uncertainty baseline presented earlier, they provide additional insight through uncertainty metrics. For instance, the same LAION CLIP ViT-H/14 ensemble model achieved a total uncertainty (TU) count of 268 and incorrect-certainty (IC) of 49, which were among the lowest in the top-performing group. This suggests a relatively low frequency of incorrect but confident predictions. Among the uncertainty-aware methods, Ensemble generally outperformed MCD and EMCD in both classification metrics and uncertainty-specific measures. For example, OpenAI CLIP ViT-L/14 with the Ensemble method reached an F1 score of 82.46% and UAcc of 74.14%, while the same model with MCD and EMCD attained lower UAcc values of 70.02% and 68.90%, respectively. However, EMCD occasionally showed better uncertainty calibration; for instance, in DenseNet121, EMCD reduced the incorrect-certainty rate (IC = 44) compared to MCD (IC = 63), even though its UAcc remained slightly lower (70.44% vs 70.84%).

The classification performance results in Table 3 compare various conventional machine learning methods combined with different feature extractors on the HAM10000 dataset. The highest classification accuracy was obtained using the Support Vector Machine (SVM) method with the LAION CLIP ViT-H/14 feature extractor, reaching 84.64% accuracy, 83.86% precision, 84.64% recall, and an F1 score of 83.48%. This same combination was also tested with another SVM configuration, achieving nearly identical results (accuracy = 84.34%, precision = 83.54%, recall = 84.44%, F1 = 83.49%), suggesting stable performance. Across all feature extractors, LAION CLIP ViT-H/14 consistently led to high classification scores when paired with multiple methods. For example, with logistic regression, it achieved 82.02% accuracy and an F1 score of 81.34%, while with XGBoost, it reached 80.94% accuracy and 80.91% recall. This demonstrates that LAION CLIP ViT-H/14 offers highly discriminative features across different classifiers. When comparing classifiers, SVM achieved the best overall performance across most feature extractors. For instance, it reached 82.41% accuracy with OpenAI CLIP ViT-L/14 and 81.56% with OpenAI CLIP ViT-B/16. Logistic regression and XGBoost also produced competitive results, especially when paired with stronger feature extractors such as OpenAI CLIP ViT-L/14 and ViT-B/16. In contrast, simpler classifiers such as KNeighbors and Naive Bayes generally showed lower performance. For instance, Naive Bayes with EfficientNet-V2-L resulted in 68.71% accuracy and 69.06% re-

call, while KNeighbors with the same extractor recorded 67.86% accuracy and 65.27% F1 score. These results confirm that SVM, when combined with high-capacity vision transformer-based features, such as LAION CLIP ViT-H/14, yields the most accurate and consistent performance for skin lesion classification in this setting.

As observed in the first phase, CLIP-based transformers, particularly those pre-trained on LAION or OpenAI datasets, consistently delivered strong performance when paired with all three uncertainty quantification methods. In contrast, feature extractors such as EfficientNet-V2-L and older CNN architectures like VGG16 and DenseNet121 tended to yield lower performance and poorer uncertainty handling. For example, EfficientNet-V2-L with EMCD achieved the lowest uncertainty accuracy despite being a deeper model, likely due to less effective representation learning for this task.

In summary, the integration of uncertainty-aware techniques into the classification framework provides valuable complementary insights to standard performance metrics. While Ensemble-based methods offer the best overall trade-off between classification performance and uncertainty handling, EMCD can be more sensitive in detecting uncertain cases. These results support the utility of combining modern feature extractors with uncertainty-aware frameworks for more transparent and trustworthy decision-making in medical imaging tasks.

3.4. Discussion

Our results reveal CLIP-based vision transformers, especially ViT-H/14 trained on LAION, consistently produced discriminative features that led to strong classification and uncertainty-aware performance. Tree-based and margin-based classifiers (e.g., XGBoost, SVM) effectively leveraged the complex feature space. Ensemble UQ methods provided a balanced trade-off between predictive accuracy and confidence, while EMCD offered better uncertainty sensitivity. In summary, combining powerful feature extractors like CLIP with appropriate classifiers and UQ methods enhances both performance and transparency, which is essential in sensitive applications like medical image analysis. The CLIP-based transformer outperformed CNNs in classifying HAM10000 images due to differences in the nature of the extracted features. While CNNs rely on convolutional operations that focus on local spatial features and were trained on natural images, the CLIP model was trained on large-scale image-text pairs, resulting in a more general and semantically rich representation. This enables the CLIP encoder to capture global context and abstract patterns, which are beneficial for medical image analysis. Additionally, the transformer ability to model long-range dependencies across image regions allows it to represent structural information more effectively. These properties likely led to more discriminative features for classification, improving both standard accuracy and uncertainty accuracy on the HAM10000 dataset.

4. Conclusion

This study presented a comprehensive evaluation of deep learning-based approaches for automated skin cancer classifica-

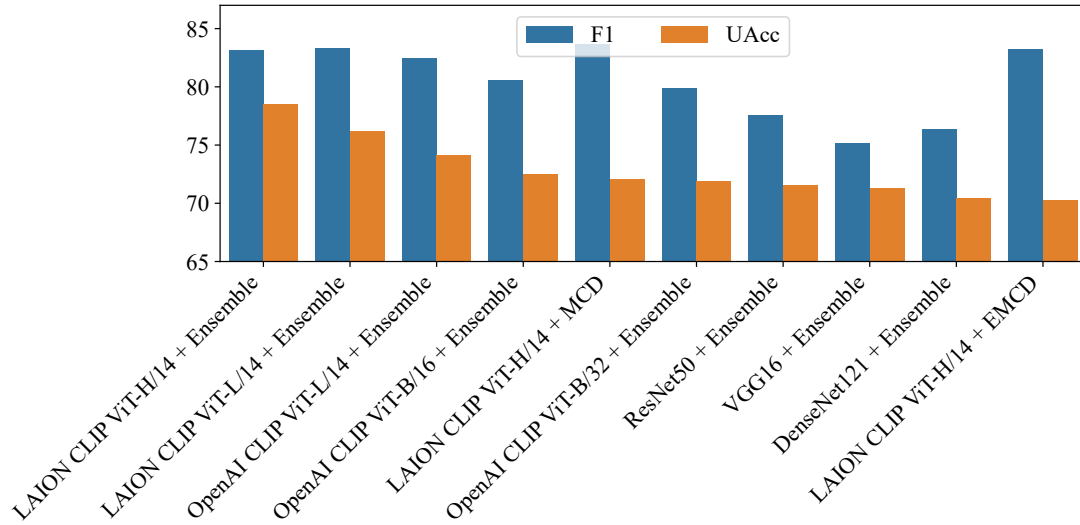


Figure 5: Performance comparison of the best-performing algorithms across various CLIP-based architectures and uncertainty-aware ensemble strategies. Evaluated metrics include Accuracy (Acc), F1 Score (F1), and Uncertainty Accuracy (UAcc). LAION CLIP ViT-H/14 + Ensemble is the Proposed method of this research has the best outcome.

tion, focusing on both classification performance and model reliability through uncertainty quantification. Several pre-trained feature extractors, including CLIP variants, ResNet50, DenseNet121, VGG16, and EfficientNet-V2-L, were used to extract representations from dermatoscopic images. These features were then classified using a diverse set of machine learning algorithms. The combination of LAION CLIP ViT-H/14 with support vector machines achieved the highest performance, demonstrating the effectiveness of contrastive language-image pre-training in skin lesion analysis. In addition to standard classification metrics, uncertainty-aware methods were employed to assess the reliability of model predictions. Techniques such as Monte Carlo Dropout, Ensemble, and Ensemble Monte Carlo Dropout were evaluated using uncertainty-specific metrics. Results indicated that ensemble-based methods offered a strong balance between classification accuracy and uncertainty awareness, while Ensemble Monte Carlo Dropout provided improved sensitivity to uncertain cases. The findings highlight the importance of selecting appropriate feature extractors and classifiers for medical image classification tasks and demonstrate the added value of incorporating uncertainty quantification. Such integration can enhance the transparency, reliability, and trustworthiness of automated diagnostic systems, contributing to safer decision-making in clinical applications.

5. Acknowledgment

Table 2: Summary of comparison of performances (%) of uncertainty-aware methods using different feature extractors on HAM10000 dataset.

Feature Extractor	Method	Acc	Pre	Recall	F1	TU	IC	CU	CC	UAcc	USen	USpe	UPre
LAION CLIP ViT-H/14*	Ensemble	84.17	83.46	84.17	83.14	268	49	381	1305	78.53	84.54	77.40	41.29
LAION CLIP ViT-L/14	Ensemble	84.42	82.62	84.42	83.32	263	49	428	1263	76.19	84.29	74.69	38.06
OpenAI CLIP ViT-L/14	Ensemble	83.62	82.82	83.62	82.46	284	44	474	1201	74.14	86.59	71.70	37.47
OpenAI CLIP ViT-B/16	Ensemble	81.78	80.82	81.78	80.58	308	57	494	1144	72.49	84.38	69.84	38.40
LAION CLIP ViT-H/14	MCD	84.52	83.71	84.52	83.69	283	27	533	1160	72.04	91.29	68.52	34.68
OpenAI CLIP ViT-B/32	Ensemble	81.43	79.34	81.43	79.91	321	51	512	1119	71.89	86.29	68.61	38.54
ResNet50**	Ensemble	79.28	77.96	79.28	77.62	363	52	517	1071	71.59	87.47	67.44	41.25
VGG16	Ensemble	77.33	74.34	77.33	75.14	408	46	529	1020	71.29	89.87	65.85	43.54
DenseNet121	Ensemble	78.73	75.83	78.73	76.38	378	48	544	1033	70.44	88.73	65.50	41.00
LAION CLIP ViT-H/14	EMCD	84.32	83.62	84.32	83.28	292	22	574	1115	70.24	92.99	66.02	33.72
OpenAI CLIP ViT-L/14	MCD	82.53	80.51	82.53	81.21	322	28	573	1080	70.00	92.00	65.34	35.98
LAION CLIP ViT-L/14	MCD	83.97	82.21	83.97	82.92	295	26	588	1094	69.35	91.90	65.04	33.41
LAION CLIP ViT-L/14	EMCD	84.27	82.42	84.27	83.11	291	24	599	1089	68.90	92.38	64.51	32.70
ResNet50	MCD	78.03	75.63	78.03	76.41	404	36	609	954	67.80	91.82	61.04	39.88
OpenAI CLIP ViT-L/14	EMCD	83.77	83.00	83.77	82.54	299	26	626	1052	67.45	92.00	62.69	32.32
OpenAI CLIP ViT-B/16	MCD	81.98	80.03	81.98	80.68	327	34	621	1021	67.30	90.58	62.18	34.49
OpenAI CLIP ViT-B/32	MCD	81.38	79.24	81.38	79.95	340	33	624	1006	67.20	91.15	61.72	35.27
OpenAI CLIP ViT-B/32	EMCD	81.38	79.28	81.38	79.81	349	24	639	991	66.90	93.57	60.80	35.32
VGG16	MCD	76.19	73.27	76.19	74.05	444	33	631	895	66.85	93.08	58.65	41.30
OpenAI CLIP ViT-B/16	EMCD	81.78	79.66	81.78	80.38	339	26	641	997	66.70	92.88	60.87	34.59
ResNet50	EMCD	79.23	76.71	79.23	77.41	384	32	653	934	65.80	92.31	58.85	37.03
VGG16	EMCD	77.18	74.01	77.18	74.82	432	25	664	882	65.60	94.53	57.05	39.42
DenseNet121	MCD	77.68	74.58	77.68	75.31	427	20	683	873	64.90	95.53	56.11	38.47
DenseNet121	EMCD	78.78	75.94	78.78	76.18	411	14	732	846	62.76	96.71	53.61	35.96
EfficientNet-V2-L	Ensemble	71.99	66.15	71.99	67.06	524	37	717	725	62.36	93.40	50.28	42.22
EfficientNet-V2-L	MCD	71.94	65.55	71.94	66.89	540	22	835	606	57.21	96.09	42.05	39.27
EfficientNet-V2-L	EMCD	71.89	65.84	71.89	66.68	543	20	855	585	56.32	96.45	40.62	38.84

Notes: * Proposed method of this research.

** The procedure that has been proposed by [2] to assess UAcc in skin cancer.

Table 3: Comparison of classification performance across various methods and feature extractors on the HAM10000 dataset.

Feature Extractor	Method	Acc	Pre	Recall	F1
LAION CLIP ViT-H/14	SVM	84.64	83.86	84.64	83.48
LAION CLIP ViT-L/14	SVM	84.44	83.54	84.44	83.29
OpenAI CLIP ViT-L/14	SVM	82.41	81.34	82.41	81.00
LAION CLIP ViT-L/14	LogisticRegression	82.16	81.15	82.16	81.46
LAION CLIP ViT-H/14	LogisticRegression	82.02	81.03	82.02	81.34
OpenAI CLIP ViT-B/16	SVM	81.76	79.61	81.76	80.08
LAION CLIP ViT-H/14	Xgboost	81.58	80.16	81.58	79.76
LAION CLIP ViT-L/14	Xgboost	80.94	79.47	80.94	79.06
OpenAI CLIP ViT-B/32	SVM	80.92	79.07	80.92	79.11
OpenAI CLIP ViT-L/14	LogisticRegression	80.62	79.36	80.62	79.77
OpenAI CLIP ViT-B/16	LogisticRegression	79.82	78.44	79.82	78.76
OpenAI CLIP ViT-B/32	LogisticRegression	79.28	77.70	79.28	78.10
OpenAI CLIP ViT-L/14	Xgboost	79.27	77.44	79.27	77.16
LAION CLIP ViT-L/14	KNeighbors	79.03	77.92	79.03	77.94
LAION CLIP ViT-H/14	KNeighbors	78.84	77.67	78.84	77.71
ResNet50	SVM	78.66	76.35	78.66	76.44
LAION CLIP ViT-H/14	GradientBoosting	78.38	75.75	78.38	76.08
OpenAI CLIP ViT-B/16	Xgboost	78.25	75.79	78.25	75.47
DenseNet121	SVM	78.10	75.36	78.10	75.62
OpenAI CLIP ViT-B/32	Xgboost	77.71	75.04	77.71	75.06
LAION CLIP ViT-L/14	GradientBoosting	77.47	74.61	77.47	74.96
OpenAI CLIP ViT-L/14	KNeighbors	76.88	75.66	76.88	75.73
VGG16	SVM	76.83	73.78	76.83	73.69
ResNet50	LogisticRegression	76.78	74.79	76.78	75.37
OpenAI CLIP ViT-L/14	GradientBoosting	76.31	73.04	76.31	73.57
ResNet50	Xgboost	76.15	73.27	76.15	73.06
DenseNet121	Xgboost	75.66	72.56	75.66	72.37
DenseNet121	LogisticRegression	75.65	73.35	75.65	74.03
OpenAI CLIP ViT-B/16	GradientBoosting	75.19	71.46	75.19	72.17
OpenAI CLIP ViT-B/32	GradientBoosting	75.10	71.68	75.10	72.10
OpenAI CLIP ViT-B/16	KNeighbors	74.84	72.90	74.84	73.20
VGG16	Xgboost	74.68	71.38	74.68	70.97
OpenAI CLIP ViT-B/32	KNeighbors	74.50	72.42	74.50	72.62
VGG16	LogisticRegression	74.36	71.47	74.36	72.28
LAION CLIP ViT-L/14	NaiveBayes	73.76	73.34	73.76	73.12
ResNet50	KNeighbors	73.45	71.96	73.45	72.06
ResNet50	GradientBoosting	73.34	69.07	73.34	69.87
LAION CLIP ViT-H/14	NaiveBayes	73.11	73.26	73.11	72.61
DenseNet121	GradientBoosting	72.98	68.58	72.98	69.34
DenseNet121	KNeighbors	72.72	70.75	72.72	71.16
LAION CLIP ViT-L/14	RandomForest	72.68	72.59	72.68	65.26
LAION CLIP ViT-H/14	RandomForest	72.67	73.29	72.67	65.11
VGG16	GradientBoosting	72.40	67.81	72.40	68.36
VGG16	KNeighbors	72.26	68.88	72.26	69.64
EfficientNet-V2-L	Xgboost	71.75	65.52	71.75	66.17
EfficientNet-V2-L	SVM	71.28	65.54	71.28	63.93
OpenAI CLIP ViT-B/16	NaiveBayes	71.13	70.51	71.13	70.22
EfficientNet-V2-L	LogisticRegression	70.88	65.90	70.88	66.86
OpenAI CLIP ViT-L/14	RandomForest	70.71	69.25	70.71	61.80
DenseNet121	RandomForest	70.41	68.13	70.41	61.68
OpenAI CLIP ViT-B/32	NaiveBayes	70.21	69.10	70.21	69.20
EfficientNet-V2-L	GradientBoosting	69.97	63.11	69.97	63.84
ResNet50	RandomForest	69.86	67.64	69.86	60.31
OpenAI CLIP ViT-B/32	RandomForest	69.85	68.70	69.85	60.06
VGG16	RandomForest	69.76	66.77	69.76	60.48
EfficientNet-V2-L	RandomForest	69.74	63.73	69.74	60.12
OpenAI CLIP ViT-B/16	RandomForest	69.50	67.82	69.50	59.31
OpenAI CLIP ViT-L/14	NaiveBayes	68.71	69.00	68.71	68.36
EfficientNet-V2-L	KNeighbors	67.86	63.69	67.86	65.27

Feature Extractor	Method	Acc	Pre	Recall	F1
ResNet50	NaiveBayes	65.31	65.38	65.31	64.87
LAION CLIP ViT-L/14	DecisionTree	64.98	65.34	64.98	65.13
LAION CLIP ViT-H/14	DecisionTree	64.72	65.04	64.72	64.85
DenseNet121	NaiveBayes	63.79	68.01	63.79	64.85
OpenAI CLIP ViT-L/14	DecisionTree	63.32	63.41	63.32	63.35
OpenAI CLIP ViT-B/16	DecisionTree	62.51	62.87	62.51	62.67
VGG16	NaiveBayes	62.40	60.72	62.40	61.00
OpenAI CLIP ViT-B/32	DecisionTree	61.92	62.28	61.92	62.07
DenseNet121	DecisionTree	61.40	61.90	61.40	61.62
ResNet50	DecisionTree	60.98	61.61	60.98	61.27
VGG16	DecisionTree	59.74	60.56	59.74	60.12
EfficientNet-V2-L	DecisionTree	56.94	57.93	56.94	57.41
EfficientNet-V2-L	NaiveBayes	32.69	60.56	32.69	36.88

References

- [1] A. F. Jerant, J. T. Johnson, C. D. Sheridan, T. J. Caffrey, Early detection and treatment of skin cancer, *American family physician* 62 (2) (2000) 357–368.
- [2] A. Shamsi, H. Asgharnezhad, Z. Bouchani, K. Jahanian, M. Saberi, X. Wang, I. Razzak, R. Alizadehsani, A. Mohammadi, H. Alinejad-Rokny, A novel uncertainty-aware deep learning technique with an application on skin cancer diagnosis, *Neural Computing and Applications* 35 (30) (2023) 22179–22188.
- [3] P. Tabarisaadi, A. Khosravi, S. Nahavandi, Uncertainty-aware skin cancer detection: The element of doubt, *Computers in Biology and Medicine* 144 (2022) 105357.
- [4] O.-J. Skrede, S. De Raedt, A. Kleppe, T. S. Hveem, K. Liestøl, J. Maddison, H. A. Askautrud, M. Pradhan, J. A. Nesheim, F. Albreghsen, et al., Deep learning for prediction of colorectal cancer outcome: a discovery and validation study, *The Lancet* 395 (10221) (2020) 350–360.
- [5] C. F. S. d. F. Mendes, R. A. Krohling, Deep and handcrafted features from clinical images combined with patient information for skin cancer diagnosis, *Chaos, Solitons & Fractals* 162 (2022) 112445.
- [6] M. Toğaçar, Z. Cömert, B. Ergen, Intelligent skin cancer detection applying autoencoder, mobilenetv2 and spiking neural networks, *Chaos, Solitons & Fractals* 144 (2021) 110714.
- [7] A. Alhudhaif, B. Almaslukh, A. O. Aseeri, O. Guler, K. Polat, A novel nonlinear automated multi-class skin lesion detection system using soft-attention based convolutional neural networks, *Chaos, Solitons & Fractals* 170 (2023) 113409.
- [8] E. Begoli, T. Bhattacharya, D. Kusnezov, The need for uncertainty quantification in machine-assisted medical decision making, *Nature Machine Intelligence* 1 (1) (2019) 20–23.
- [9] M. Abdar, F. Pourpanah, S. Hussain, D. Rezazadegan, L. Liu, M. Ghavamzadeh, P. Fieguth, X. Cao, A. Khosravi, U. R. Acharya, et al., A review of uncertainty quantification in deep learning: Techniques, applications and challenges, *Information fusion* 76 (2021) 243–297.
- [10] G. Litjens, T. Kooi, B. E. Bejnordi, A. A. A. Setio, F. Ciompi, M. Ghafoorian, J. A. Van Der Laak, B. Van Ginneken, C. I. Sánchez, A survey on deep learning in medical image analysis, *Medical image analysis* 42 (2017) 60–88.
- [11] V. Cheplygina, M. De Bruijne, J. P. Pluim, Not-so-supervised: a survey of semi-supervised, multi-instance, and transfer learning in medical image analysis, *Medical image analysis* 54 (2019) 280–296.
- [12] H. Greenspan, B. Van Ginneken, R. M. Summers, Guest editorial deep learning in medical imaging: Overview and future promise of an exciting new technique, *IEEE transactions on medical imaging* 35 (5) (2016) 1153–1159.
- [13] A. Esteva, B. Kuprel, R. A. Novoa, J. Ko, S. M. Swetter, H. M. Blau, S. Thrun, Dermatologist-level classification of skin cancer with deep neural networks, *nature* 542 (7639) (2017) 115–118.
- [14] H.-C. Shin, H. R. Roth, M. Gao, L. Lu, Z. Xu, I. Nogues, J. Yao, D. Mollura, R. M. Summers, Deep convolutional neural networks for computer-aided detection: Cnn architectures, dataset characteristics and transfer learning, *IEEE transactions on medical imaging* 35 (5) (2016) 1285–1298.
- [15] N. Tajbakhsh, J. Y. Shin, S. R. Gurudu, R. T. Hurst, C. B. Kendall, M. B. Gotway, J. Liang, Convolutional neural networks for medical image analysis: Full training or fine tuning?, *IEEE transactions on medical imaging* 35 (5) (2016) 1299–1312.
- [16] J. Yosinski, J. Clune, Y. Bengio, H. Lipson, How transferable are features in deep neural networks?, *Advances in neural information processing systems* 27 (2014).
- [17] K. He, X. Zhang, S. Ren, J. Sun, Deep residual learning for image recognition, in: *Proceedings of the IEEE Conference on Computer Vision and Pattern Recognition (CVPR)*, 2016, pp. 770–778.
- [18] G. Huang, Z. Liu, L. Van Der Maaten, K. Q. Weinberger, Densely connected convolutional networks, in: *Proceedings of the IEEE Conference on Computer Vision and Pattern Recognition (CVPR)*, 2017, pp. 4700–4708.
- [19] K. Simonyan, A. Zisserman, Very deep convolutional networks for large-scale image recognition, *International Conference on Learning Representations (ICLR)* (2015). [arXiv:1409.1556](https://arxiv.org/abs/1409.1556).
- [20] M. Tan, Q. V. Le, Efficientnetv2: Smaller models and faster training, in: *Proceedings of the 38th International Conference on Machine Learning (ICML)*, 2021, pp. 10096–10106.
- [21] A. Radford, J. W. Kim, C. Hallacy, A. Ramesh, G. Goh, S. Agarwal, G. Sasstry, A. Askell, P. Mishkin, J. Clark, et al., Learning transferable visual models from natural language supervision, in: *International conference on machine learning*, PMLR, 2021, pp. 8748–8763.
- [22] B. Lakshminarayanan, A. Pritzel, C. Blundell, Simple and scalable predictive uncertainty estimation using deep ensembles, *Advances in neural information processing systems* 30 (2017).
- [23] Y. Gal, Z. Ghahramani, Dropout as a bayesian approximation: Representing model uncertainty in deep learning, in: *international conference on machine learning*, PMLR, 2016, pp. 1050–1059.
- [24] P. Tabarisaadi, A. Khosravi, S. Nahavandi, M. Shafie-Khah, J. P. Catalão, An optimized uncertainty-aware training framework for neural networks, *IEEE transactions on neural networks and learning systems* 35 (5) (2022) 6928–6935.
- [25] P. Tschandl, C. Rosendahl, H. Kittler, The ham10000 dataset, a large collection of multi-source dermatoscopic images of common pigmented skin lesions, *Scientific data* 5 (1) (2018) 1–9.
- [26] I. T. Jolliffe, J. Cadima, Principal component analysis: a review and recent developments, *Philosophical Transactions of the Royal Society A: Mathematical, Physical and Engineering Sciences* 374 (2065) (2016) 20150202.